Steel and Composite Structures, *Vol. 36, No. 4* (*2020*) *481-492*
DOI: https://doi.org/10.12989/scs.2020.36.4.481

Mapped relationships between pier settlement and rail deformation of bridges with CRTS III SBT

Lizhong Jiang[1,2a], Lili Liu[1b], Wangbao Zhou*[1], Xiang Liu[1c], Chao Liu[1d] and Ping Xiang[1e]

[1]*School of Civil Engineering, Central South University, Changsha 410075, China*
[2]*National Engineering Laboratory for High Speed Railway Construction, Changsha 410075, China*

(*Received December 19, 2019, Revised July 28, 2020, Accepted August 8, 2020*)

Abstract. To study the rail mapped deformation caused by the pier settlement of simply - supported bridges with China Railway Track System III (CRTS III) slab ballastless track (SBT) system under the mode of non-longitudinal connection ballastless track slab, this study derived an analytical solution to the mapped relationships between pier settlement and rail deformation based on the interlayer interaction mechanism of rail-pier and principle of stationary potential energy. The analytical calculation results were compared with the numerical results obtained by ANSYS finite element calculation, thus verifying the accuracy of analytical method. A parameter analysis was conducted on the key factors in rail mapped deformation such as pier settlement, fastener stiffness, and self-compacting concrete (SCC) stiffness of filling layer. The results indicate that rail deformation is approximately proportional to pier settlement. The smaller the fastener stiffness, the smoother the rail deformation curve and the longer the rail deformation area is. With the increase in the stiffness of SCC filling layer, the maximum positive deformation of rail gradually decreases, and the maximum negative deformation gradually increases. The deformation of rail caused by the pier settlement of common-span bridge structures will generate low-frequency excitation on high-speed trains.

Keywords: pier settlement; CRTS III SBT system; geometrical morphology of rail surface; mapped relationships; principle of stationary potential energy; subgrade

1. Introduction

Because of geological conditions, environment and other factors, “replacing road with bridge” design concept has been widely applied, therefore, a bridge structure has become one of the main parts in high-speed railway lines. CRTS III SBT system has the advantages of CRTS I and CRTS II SBT system, optimizes and integrates the existing ballastless track, and has been widely used in high-speed railway systems at present. However, with the rapid expansion in the coverage area of high-speed railway networks, the mileage of high-speed railway in special areas such as active seismic zones and those with foundation settlement and extreme climate is becoming increasingly longer, and the bridge structure will inevitably generate uneven settlement. The uneven settlement will sink the beam, leading to rail deformation through the coupling interaction between bridge and rail. As a train passes at a high speed, the deformation will increase the excitation on wheel-rail interface and then intensify the train’s vibration, which will affect the running stability and riding comfort of trains and even might cause derailment in serious cases. Therefore, study of the mapped relationships between pier settlement and rail deformation is an important prerequisite to evaluate the effects of pier settlement on the running safety and stability of high-speed trains.

Many studies have been reported on the coupling vibration of vehicles and bridges. In the literature (Al Shaer *et al*. 2008, Wang *et al*. 2015, Zhai *et al*. 2015), to study the dynamic response characteristics of high-speed trains to the ground or track system, field tests and experimental studies were carried out. A train-track-bridge refined finite element model has been established (Shan *et al*. 2013, Wang *et al*. 2013), and the dynamic interaction between vehicles and bridges under earthquake has been analyzed. Yang *et al*. (2017) conducted a comprehensive study on vehicle-bridge resonance and bridge-bridge resonance in vehicle-bridge system using a combination of analytical method and finite element method, the results show that the bridge resonates when the train is running at a high speed, and the train compartment resonates when the train is running at a low speed. Xia *et al*. (2006) studied the resonance mechanism and resonance conditions of train-bridge system by theoretical derivation, numerical simulation, and experimental data analysis, the results show that the

*Corresponding author, Professor
E-mail: zhouwangbao@163.com
[a]Professor
E-mail: lzhjiang@csu.edu.cn
[b]Ph.D. Student
E-mail: liulily2019@csu.edu.cn
[c]Ph.D. Student
E-mail: liuxiang2017@csu.edu.cn
[d]Student
E-mail: liu97chao@csu.edu.cn
[e]Professor
E-mail: pxiang2-c@my.cityu.edu.hk

ISSN: 1229-9367 (Print), 1598-6233 (Online)

resonance of train-bridge system is affected by the span, total length, lateral and vertical stiffness of the bridge, compositions of trains, axle arrangements and natural frequencies of vehicles. Because the response of superstructure is closely related to the deformation of substructure, a large number of long-term observations have been conducted on the settlement of the bridge structural foundation and pier (Niu *et al*. 2011, Yang *et al*. 2014). Settlement is a long-term accumulation process. Long-term observation is time-consuming and labor-intensive, and the data obtained are only for an existing structure. Therefore, an autoregressive model is proposed to predict the settlement of high-speed railway piers (Gong and Li. 2016, Liu *et al*. 2019). Based on settlement observation, further studies have been conducted. For example, Paixão *et al*. (2015) studied the effect of uneven settlement on the dynamic response of train-track system by establishing a finite element model and using nonlinear dynamic analysis method. The ANSYS finite element model by the theoretical analysis of train-track-bridge coupling interaction and studied the effect of settlement pier on the running safety of high-speed trains has been established (Biondi *et al*. 2005, Lee *et al*. 2012, Doménech *et al*. 2014, Toydemir *et al*. 2017). It was concluded that speed is the main factor affecting the safety and stability of high-speed trains in the case of local land subsidence. Yau (2009) proposed an incremental iterative method to solve the train vibration problem of beam structure under support settlement. Numerical studies show that for the dynamic interaction of vehicle-bridge system, the effect of land subsidence on the bridge response is generally small, but it has a large amplification effect on the vertical response of moving trains. This conclusion is important for the railway line crossing the land subsidence area. In the literature (Xiong *et al*. 2006, Ahmari *et al*. 2015), the dynamic interaction between vehicle and bridge structure was studied when the supporting structure subsides, which was consistent with the above research conclusions. Ju (2013) established a three-dimensional nonlinear finite element model based on factors such as rail irregularities, track–bridge interactions and wheel-rail separations. The results show that the settlement or rotation of foundation will cause huge displacements between the two simply - supported girders, resulting in a large train derailment coefficient that threatens traffic safety. Because of the serious harm of settlement, some settlement limits have been obtained through many studies (Chen *et al*. 2018, Yan *et al*. 2018). In recent years, studies on the mechanism of dynamic response change of vehicle-bridge caused by settlement have become more and more detailed. For example, the effect of subgrade settlement on the structural performance of bridge and culvert panels has been studied in the literature (Rocha *et al*. 2015, Guan *et al*. 2019, Jiang *et al*. 2019, Jiang *et al*. 2019). In the literature (Jahangiri and Zakeri 2017, Erol 2018) the effects of vertical deformation of pier on the deflection of main beam and the effects of lateral deformation of bridge on the track geometry have been studied. The parameters affecting the deformation of rail such as the deformation amplitude, fastener stiffness and stiffness of structural layer have been obtained. Gou *et al*. (2019) deduced an analytical solution of mapped relationships between the deformation of high-speed railway overpass and track geometry and used the analytical solution to quantitatively analyze the influencing parameters. The study shows that rail deflection increases with the magnitude of bridge pier settlement and vertical girder fault. Increasing the stiffness of fasteners or mortar layer tends to cause a steep rail deformation curve, undesired for the running safety and riding comfort of high-speed railway. Indraratna *et al*. (2014) studied the mapped relationships between geometric deformation and additional stress of ballastless track structure caused by subgrade differential settlement under self-weight loads in high-speed railway. The conclusions are consistent with Gou's conclusions.

To sum up, pier settlement is one of the key factors affecting the running stability and safety of high-speed railway trains. Study of interlayer interaction mechanism of bridge-track system and rail mapped deformation caused by pier settlement has great theoretical and practical significance in the integrated management of static and dynamic performance of rail line operation safety. At present, the mapped relationships between pier settlement and rail deformation for CRTS III SBT -bridge system have been rarely studied. This study considered multispan simply - supported bridge with CRTS III SBT system as the research object, an analytical solution to the mapped relationships between pier settlement and rail deformation was derived based on the principle of stationary potential energy, and ANSYS finite element model was established to verify the accuracy of analytical solution. Finally, for the track surface under pier settlement, a parametric analysis was conducted on the influencing factors for the variation of geometrical morphology.

2. Mapped relationships between linear change in beam and rail deformation

2.1 Mechanism analysis on rail deformation caused by pier settlement

The main components of CRTS III SBT structure include ordinary 60 track, WJ-8C fastener system, bidirectional prestressed reinforced concrete prefabricated track slab, SCC filling layer, and reinforced concrete base slab (the subgrade section is hydraulic bearing layer) (Cai *et al*. 2005). The connection between track slab and SCC filling layer is strengthened by setting U-shaped connecting rebar. Two downward convex platforms are set at the ends of SCC filling layer, and two upward grooves are set at the ends of reinforced concrete base slab to connect to the SCC filling layer. On the inner side of groove, a 10-mm-thick rubber backing plate is closely clung, at the bottom, a 20-mm-thick foam board is laid. A geotextile of 4 mm thickness is laid between the base slab and SCC filling layer. Fig. 1 shows a schematic diagram of the structure of CRTS III SBT.

According to the structure of CRTS III SBT and its laying mode of non-longitudinal connection ballastless track slab,

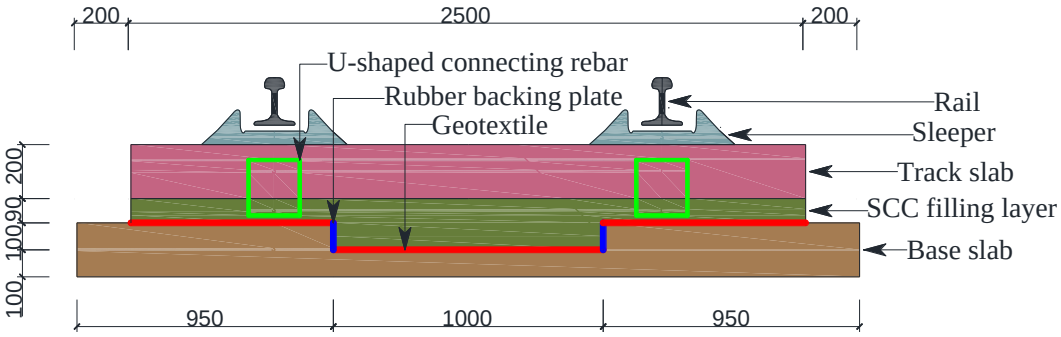

Fig. 1 Schematic diagram of the structure of CRTS III SBT.

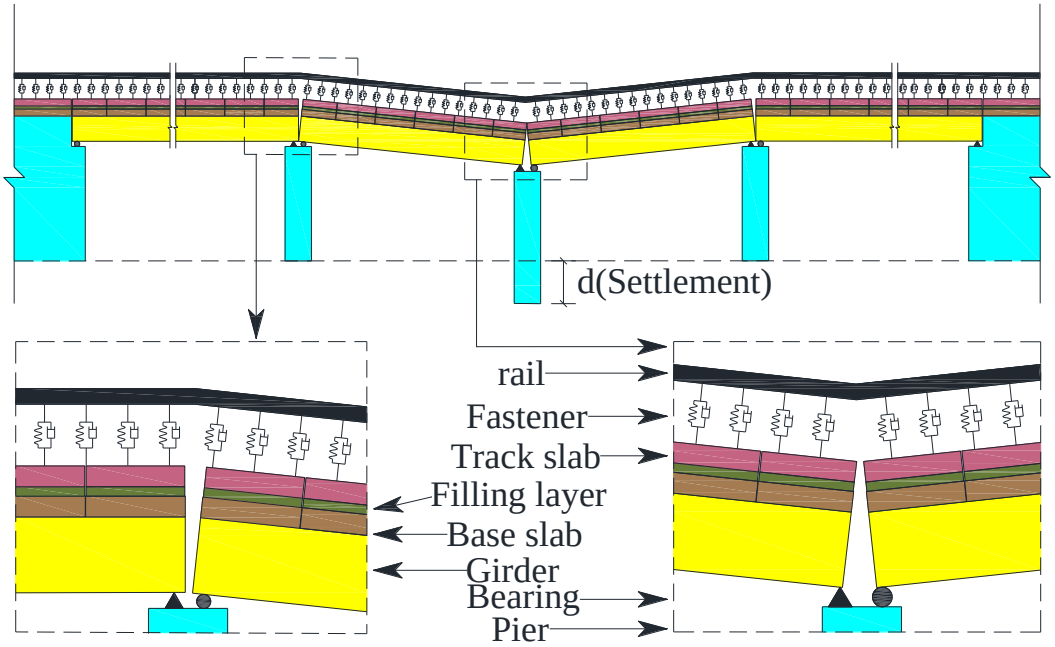

Fig. 2 The mapped deformation of rail with pier settlement in CRTS III SBT- simply - supported bridge system.

when the pier of simply - supported bridge suffers from settlement, the two-span beam adjacent to the settlement pier will suffer vertical deformation due to the action of gravity. The base slab laid on the girder will suffer collaborative deformation with the girder under the action of gravity and tension of embedded rebars. Rail and unit track slab suffer subsequent vertical deformation under the action of gravity and interlayer components. Fig. 2 shows the mapped deformation of rail with pier settlement in CRTS III SBT - simply - supported bridge system.

2.2 Basic hypothesis

To establish a simplified calculation model for the mapped relationships between pier settlement and rail deformation of CRTS III SBT - bridge system, the following basic hypotheses are made:

(1) When a force analysis is conducted on the system, the gravity balance state of system is taken as the initial state, and gravity is neglected in the calculation process.

(2) The connection between base slab and girder by embedded rebars has a stronger interlayer constraint effect; therefore, it is hypothesized that the base slab and girder deform coordinately.

(3) The vertical flexural stiffness of a bridge is much greater than that of a track system, and the effect of rail on the deformation of bridge structure is neglected.

(4) The rail in subgrade section can be simplified as the simply supported boundary, and the boundary effect of rail within the subgrade section can be eliminated using enough calculation length of subgrade section.

(5) The fasteners are considered as linear discrete springs along the centerline of rail, and the SCC filling layer are considered as Winker linear springs along the centerline of rail.

2.3 Basic equations of mapped relationships

It is hypothesized that the number of track slabs in the entire bridge-track system is M. Six track slabs are laid

out on the standard simply - supported of each span and the subgrades at both ends, and there are N fasteners on each track slab. Thus, there are MN fasteners and $M/6-2$ span simply - supported in total.

2.3.1 Rail displacement

As a pier suffers from settlement, the vertical deformation of rail with pier settlement is denoted as ω_1. Then, the simply supported boundary condition of rail can be expressed as

$$\begin{aligned} &\omega_{1(x=0)}=0, \quad \omega_{1(x=l_g)}=0 \\ &\omega_1''_{(x=0)}=0, \quad \omega_1''_{(x=l_g)}=0 \end{aligned} \tag{1}$$

Where l_g is the total length of rail.

Taking sine function as the primary function, the deformation curve of rail with pier settlement can be approximately expressed as

$$\omega_1(x)=\sum_{m=1}^{n} A_m \sin(\frac{m\pi x}{l_g}) \tag{2}$$

Where $A_{\mathrm{m}}(\mathrm{m}=1,\ldots,\mathrm{n})$ denotes arbitrary constants.

The total potential energy of rail under the fastener force can be expressed as

$$\Pi=\frac{E_g I_g}{2}\int_0^{l_g}(\frac{d^2\omega_1(x)}{dx^2})^2 dx-\sum_{i=1}^{MN}\frac{1}{2}F_i\omega_1(x_i) \tag{3}$$

Where $F_i(i=1,2,\ldots\ldots,MN)$ is the fastener force; E_g is the elastic modulus of rail; I_g is the equivalent section moment of inertia of rail.

According to Rayleigh-Ritz method, $\frac{\partial\Pi}{\partial A_m}=0$

$$\frac{E_g I_g \pi^4}{2l_g^3}m^4 A_m-\sum_{i=1}^{MN}F_i\sin\frac{m\pi x_i}{l_g}=0 \tag{4}$$

Thus

$$\begin{aligned} &A_m=\frac{2l_g^3}{E_g I_g \pi^4 m^4}\sum_{i=1}^{MN}F_i\sin\frac{m\pi x_i}{l_g} \\ &(m=1,2,\ldots\ldots,n) \end{aligned} \tag{5}$$

Substituting Eq. (5) into Eq. (2)

$$\begin{aligned} &\omega_1(x_j)=\sum_{i=1}^{MN}F_i\sum_{m=1}^{n}\frac{2l_g^3}{E_g I_g \pi^4 m^4}\sin\frac{m\pi x_i}{l_g} \\ &\sin(\frac{m\pi x_j}{l_g})(j=1,2,\ldots\ldots,MN) \end{aligned} \tag{6}$$

Eq. (6) can be expressed in matrix form

$$\mathbf{\Omega_1}=\mathbf{A}\cdot\mathbf{F} \tag{7}$$

$$\mathbf{A}=\begin{bmatrix} a_{11} & \cdots & a_{1,MN} \\ \vdots & \ddots & \vdots \\ a_{MN,1} & \cdots & a_{MN,MN} \end{bmatrix} \tag{8}$$

$$a_{ij}=\sum_{m=1}^{n}\frac{2l_g^3}{E_g I_g \pi^4 m^4}\sin\frac{m\pi x_i}{l_g}\sin(\frac{m\pi x_j}{l_g}) \tag{9}$$

Where $\mathbf{F}$ is the array of fastener force; $\mathbf{\Omega_1}$ is the rail displacement array in all fastener positions; $\mathbf{A}$ is the influencing coefficient matrix of fastener force on rail displacement.

2.3.2 Beam displacement

Supposing that k^{th} pier suffers settlement, the displacement function $\omega_{2,k,k}$ of k^{th} span beam (the left span of settlement pier) can be expressed as

$$\omega_{2,k,k}(x)=\frac{x-k(l_l+s_l)}{l_l}d \tag{10}$$

And the displacement function $\omega_{2,k,k+1}$ of $(k+1)^{th}$ span beam (the right span of settlement pier) can be expressed as

$$\omega_{2,k,k+1}(x)=\frac{(k+2)\ l_l+(k+1)s_l-x}{l_l}d \tag{11}$$

According to Eqs. (10) and (11), the displacement array of girder at the corresponding fastener position can be expressed as

$$\mathbf{\Omega_2}=\mathbf{H}\cdot d \tag{12}$$

Where l_l is the length of a single-span beam; d is the pier settlement; $\mathbf{H}$ is the influencing coefficient array of settlement on bridge displacement; s_l is the beam spacing.

2.3.3 Track slab displacement

Considering the single track slab as a free beam structure and taking trigonometric function as the primary function, the function of track slab displacement $\omega_3(x)$ can be approximately expressed as

$$\begin{aligned} &\omega_3(x)=\sum_{m=1}^{n}B_m\sin(\frac{2m\pi x}{l_b}) \\ &+\sum_{m=1}^{n}C_m\cos(\frac{2m\pi x}{l_b})+D+\omega_2(x) \end{aligned} \tag{13}$$

Where $B_{\mathrm{m}}(\mathrm{m}=1,\ldots,\mathrm{n})$, $C_{\mathrm{m}}(\mathrm{m}=1,\ldots,\mathrm{n})$ and D

are arbitrary constants.

Taking the settlement of first pier as an example, then $\omega_{3,7}$, the displacement function of first track slab on the left of first-span beam (it is the 7^{th} track slab in the whole) can be expressed as

$$\begin{aligned}\omega_{3,7}(x)=&\sum_{m=1}^{n}B_{m,7}\sin\left[\frac{2m\pi\left(x-6l_b'\right)}{l_b}\right]\\&+\sum_{m=1}^{n}C_{m,7}\cos\left[\frac{2m\pi\left(x-6l_b'\right)}{l_b}\right]+D+\omega_{2,1,1}\end{aligned}\tag{14}$$

Where $l_b'=l_b+s_b$; l_b is the length of a single track slab; x is the local coordinates with the left end of a track slab as the coordinate origin; s_b is the slab spacing.

In the bridge section, the track slab is under the combined action of fastener force and spring force in the SCC filling layer, and the total potential energy of track slab can be expressed as

$$\begin{aligned}\Pi=&\frac{E_bI_b}{2}\int_0^{l_b}\left(\frac{d^2\omega_3(x)}{dx^2}\right)^2dx-\sum_{i=6N+1}^{7N}-\frac{1}{2}F_i\omega_3(x_i)\\&-\int_0^{l_b}\frac{1}{2}\omega_3(x)Q_2(x)dx\\=&\frac{4E_bI_b\pi^4}{l_b^{\,3}}\sum_{m=1}^{n}m^4\left(B_{m,7}^2+C_{m,7}^2\right)\\&+\frac{1}{2}\sum_{i=6N+1}^{7N}F_i\frac{d}{l_l}\left[x-(l_l+s_l)\right]+\frac{1}{2}\sum_{i=6N+1}^{7N}F_iD\\&+\frac{1}{2}\sum_{i=6N+1}^{7N}F_i\left[\begin{array}{l}\sum_{m=1}^{n}B_{m,7}\sin\frac{2m\pi\left(x-6l_b'\right)}{l_b}\\+\sum_{m=1}^{n}C_{m,7}\cos\frac{2m\pi\left(x-6l_b'\right)}{l_b}\end{array}\right]\\&-\frac{1}{2}\int_0^{l_b}Q_2(x)\left[\begin{array}{l}\sum_{m=1}^{n}B_{m,7}\sin\frac{2m\pi\left(x-6l_b'\right)}{l_b}\\+\sum_{m=1}^{n}C_{m,7}\cos\frac{2m\pi\left(x-6l_b'\right)}{l_b}\end{array}\right]dx\\&-\frac{1}{2}\int_0^{l_b}Q_2(x)\frac{d}{l_l}\left[x-(l_l+s_l)\right]dx-\frac{1}{2}\int_0^{l_b}Q_2(x)Ddx\end{aligned}\tag{15}$$

Where E_b is the elastic modulus of track slab; I_b is the equivalent section moment of inertia of track slab; $Q_2(x)$ is the Winker spring distribution force within the filling layer of bridge section; λ is the stiffness of Winker spring within the filling layer.

According to the moment balance of track slab

$$\int_0^{l_b}Q_2(x)\left[x-(l_l+s_l)\right]dx=\sum_{i=6N+1}^{7N}F_i\left[x-(l_l+s_l)\right]\tag{16}$$

According to the vertical force balance of track slab

$$\int_0^{l_b}Q_2(x)dx=\sum_{i=6N+1}^{7N}F_i\Rightarrow D=-\frac{\sum_{i=6N+1}^{7N}F_i}{\lambda l_b}\tag{17}$$

Substituting Eqs. (16) and (17) into Eq. (15)

$$\begin{aligned}\Pi=&\frac{4E_bI_b\pi^4}{l_b^{\,3}}\sum_{m=1}^{n}m^4\left(B_{m,7}^2+C_{m,7}^2\right)\\&+\frac{1}{2}\sum_{i=6N+1}^{7N}F_i\left[\begin{array}{l}\sum_{m=1}^{n}B_{m,7}\sin\frac{2m\pi\left(x-6l_b'\right)}{l_b}\\+\sum_{m=1}^{n}C_{m,7}\cos\frac{2m\pi\left(x-6l_b'\right)}{l_b}\end{array}\right]\\&-\frac{1}{2}\int_0^{l_b}Q_2(x)\left[\begin{array}{l}\sum_{m=1}^{n}B_{m,7}\sin\frac{2m\pi\left(x-6l_b'\right)}{l_b}\\+\sum_{m=1}^{n}C_{m,7}\cos\frac{2m\pi\left(x-6l_b'\right)}{l_b}\end{array}\right]dx\end{aligned}\tag{18}$$

According to Rayleigh-Ritz method, $\frac{\partial\Pi}{\partial B_{m,7}}=0$

$$B_{m,7}=-\frac{\sum_{i=6N+1}^{7N}\left[F_i\sin\frac{2m\pi\left(x-6l_b'\right)}{l_b}\right]}{\frac{8E_bI_b\pi^4m^4}{l_b^{\,3}}+\frac{1}{2}\lambda l_b}\tag{19}$$

$$(m=1,2,\ldots\ldots,n)$$

According to Rayleigh-Ritz method, $\frac{\partial\Pi}{\partial C_{m,7}}=0$

$$C_{m,7}=-\frac{\sum_{i=6N+1}^{7N}\left[F_i\cos\frac{2m\pi\left(x-6l_b'\right)}{l_b}\right]}{\frac{8E_bI_b\pi^4m^4}{l_b^{\,3}}+\frac{1}{2}\lambda l_b}\tag{20}$$

$$(m=1,2,\ldots\ldots,n)$$

Similarly, for p^{th} track slab

$$B_{m,p} = -\frac{\sum_{i=pN-N+1}^{pN}\left[F_i \sin\frac{2m\pi\left(x-pl_b'\right)}{l_b}\right]}{\frac{8E_bI_b\pi^4m^4}{l_b^3}+\frac{1}{2}\lambda l_b} \quad (21)$$

$(m=1,2,\ldots\ldots,n)$

$$C_{m,p} = -\frac{\sum_{i=pN-N+1}^{pN}\left[F_i \cos\frac{2m\pi\left(x-pl_b'\right)}{l_b}\right]}{\frac{8E_bI_b\pi^4m^4}{l_b^3}+\frac{1}{2}\lambda l_b} \quad (22)$$

$(m=1,2,\ldots\ldots,n)$

Substituting Eqs. (17), (21) and (22) into Eq. (13)

$$\omega_{3.p}(x_j) = -\frac{\sum_{i=pN-N+1}^{pN}F_i}{\lambda l_b}+\omega_2(x) - \sum_{i=pN-N+1}^{pN}F_i\sum_{m=1}^{n}\frac{\sin\frac{2m\pi\left(x_i-pl_b'\right)}{l_b}\sin\frac{2m\pi\left(x_j-pl_b'\right)}{l_b}}{\frac{8E_bI_b\pi^4m^4}{l_b^3}+\frac{1}{2}\lambda l_b} - \sum_{i=pN-N+1}^{pN}F_i\sum_{m=1}^{n}\frac{\cos\frac{2m\pi\left(x_i-pl_b'\right)}{l_b}\cos\frac{2m\pi\left(x_j-pl_b'\right)}{l_b}}{\frac{8E_bI_b\pi^4m^4}{l_b^3}+\frac{1}{2}\lambda l_b} \quad (23)$$

Eq. (23) can be expressed in the matrix form

$$\mathbf{\Omega_{3.p}} = \mathbf{B_p}\cdot\mathbf{F_p}+\mathbf{C_p}\cdot\mathbf{F_p}-\frac{\mathbf{E}}{\lambda l_b}\cdot\mathbf{F_p}+\mathbf{\Omega_{2,p}} \quad (24)$$

Where

$$\mathbf{B_p} = \begin{bmatrix} b_{pN-N+1,pN-N+1} & \cdots & b_{pN-N+1,pN} \\ \vdots & \ddots & \vdots \\ b_{pN,pN-N+1} & \cdots & b_{pN,pN} \end{bmatrix} \quad (25)$$

$$b_{ij} = \sum_{m=1}^{n} -\frac{\sin\frac{2m\pi\left(x_i-pl_b'\right)}{l_b}\cdot\sin\frac{2m\pi\left(x_j-pl_b'\right)}{l_b}}{\frac{8E_bI_b\pi^4m^4}{l_b^3}+\frac{1}{2}\lambda l_b} \quad (26)$$

$$\mathbf{C_p} = \begin{bmatrix} c_{pN-N+1,pN-N+1} & \cdots & c_{pN-N+1,pN} \\ \vdots & \ddots & \vdots \\ c_{pN,pN-N+1} & \cdots & c_{pN,pN} \end{bmatrix} \quad (27)$$

$$c_{ij} = \sum_{m=1}^{n} -\frac{\cos\frac{2m\pi\left(x_i-pl_b'\right)}{l_b}\cdot\cos\frac{2m\pi\left(x_j-pl_b'\right)}{l_b}}{\frac{8E_bI_b\pi^4m^4}{l_b^3}+\frac{1}{2}\lambda l_b} \quad (28)$$

The relationships matrix **B**, **C** for the effect of fastener force on track slab can be expressed as

$$\mathbf{B} = \begin{bmatrix} \mathbf{B_1} & \mathbf{0} & \cdots & \cdots & \mathbf{0} \\ \mathbf{0} & \ddots & & \mathbf{0} & \vdots \\ \vdots & & \mathbf{B_p} & & \vdots \\ \vdots & \mathbf{0} & & \ddots & \mathbf{0} \\ \mathbf{0} & \cdots & \cdots & \mathbf{0} & \mathbf{B_M} \end{bmatrix} \quad (29)$$

$$\mathbf{C} = \begin{bmatrix} \mathbf{C_1} & \mathbf{0} & \cdots & \cdots & \mathbf{0} \\ \mathbf{0} & \ddots & & \mathbf{0} & \vdots \\ \vdots & & \mathbf{C_p} & & \vdots \\ \vdots & \mathbf{0} & & \ddots & \mathbf{0} \\ \mathbf{0} & \cdots & \cdots & \mathbf{0} & \mathbf{C_M} \end{bmatrix} \quad (30)$$

The displacement matrix for track slab in all fastener positions can be expressed as

$$\mathbf{\Omega_3} = \mathbf{B}\cdot\mathbf{F}+\mathbf{C}\cdot\mathbf{F}-\frac{\mathbf{E}}{\lambda l_b}\cdot\mathbf{F}+\mathbf{\Omega_2} \quad (31)$$

For the subgrade section, the foundation deformation of subgrade section can be simulated by the stiffness of equivalent Winker spring, and then the distributed force of equivalent Winker spring $Q_1(x)$ can be expressed as

$$Q_1(x) = k_{tu}\omega_2(x) \quad (32)$$

Where k_{tu} is the stiffness of equivalent Winker spring for the foundation deformation of subgrade section.

In the subgrade section, track slab is under the combined action of fastener force and spring force on subgrade, and the solving process for the deformation of track slab in subgrade section is similar to that in bridge section.

2.3.4 Analytical expression for mapped relationships

Let k_s be the equivalent stiffness of fastener, i^{th} fastener force can be expressed as

$$F_i = k_s\left[\omega_3(x_i)-\omega_1(x_i)\right] \quad (33)$$

The fastener force can be expressed in array form as

$$\mathbf{F}=k_s\left(\mathbf{\Omega_3}-\mathbf{\Omega_1}\right) \tag{34}$$

Combining Eqs. (7), (31) and (34), the fastener force array can be expressed as a single-value function of settlement

$$\mathbf{F}=\left(\mathbf{A}+\frac{\mathbf{E}}{k_s}-\mathbf{B}-\mathbf{C}+\frac{\mathbf{E}}{\lambda l_b}\right)^{-1}\mathbf{H}\cdot d \tag{35}$$

Where $\mathbf{E}$ is the unit matrix with the same order as $\mathbf{A}$, $\mathbf{B}$ and $\mathbf{C}$.

Substituting Eq. (35) into Eq. (7), the mapped deformation of rail with pier settlement can be obtained

3. Comparisons between the analytical solution to mapped relationships and the numerical solution given by finite element model

Using ANSYS finite element software, a finite element model of six-span railway simply - supported bridge with CRTS III SBT system was established, where the rail, track slab, beam, and pier were simulated using BEAM 3 element, and the fastener, SCC filling layer, and support were simulated using COMBINE 14 spring element, and the pier settlement was simulated by applying vertical displacement to the node at the bottom of pier. An actual section parameter of 60 kg/m rail was taken. The equivalent spring stiffness of the fastener was 35 kN/mm. The equivalent spring stiffness of SCC filling layer was 1800 kN/mm. The concrete strength grade of track slab was C60. The concrete strength grade of base slab was C40. The concrete strength grade of girder was C50. The concrete strength grade of pier was C30. The beam spacing was 20 mm, and the spacing between track slab was 70 mm. The material and geometric parameters of different components of the system are summarized in Table 1.

The calculation flowchart of the proposed analytical method is shown in Fig. 3. The main parameters of the analytical model are as follows: the span of simply - supported is 32 m, the number of spans is 6, and the SBT spacing is 70 mm, as shown in Table 1 for detailed parameters.

Using the finite element model and analytical expression for rail deformation with pier settlement, the deformation curves for rail with pier settlement under various working cases were calculated. As shown in Fig. 4, in case 1, the middle pier, i.e., the 3rd pier, suffers a settlement of 5 mm. In case 2, the 2nd pier suffers a settlement of 5 mm, and the 3rd pier suffers a settlement of 3 mm.

Using analytical model and ANSYS finite element model, calculations were conducted on the deformation curve of rail with pier settlement in cases 1 and 2, and the calculation results are shown in Fig. 5. In the case of single-pier settlement and multipier settlement, the peak value on analytical model, with the difference between the two peaks less than 1‰. The slight difference indicates that the calculation curves for the finite element model and the

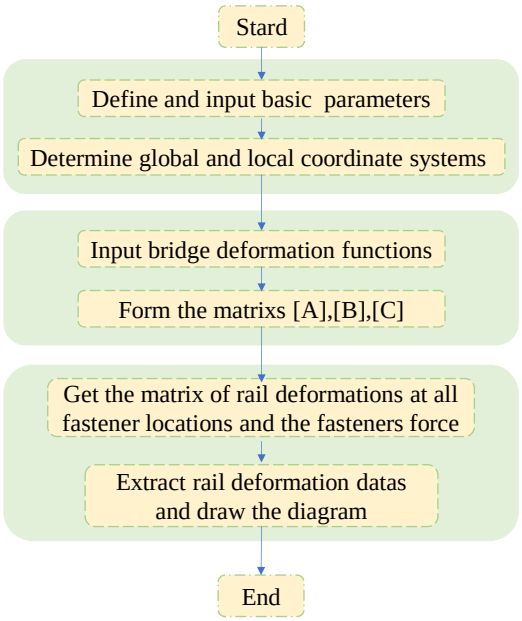

Fig. 3 The calculation flowchart of the analytical calculation model

analytical model are consistent, verifying the accuracy of analytical method and indicating that both the models can be used to calculate the mapped deformation of rail with pier settlement. Because of pier settlement, the rail suffers significant deformation. Within the settlement area, the rail suffers subsequent deformation with pier settlement. In the area far from settlement area, the rail deformation shows the decaying trend of small fluctuation. When entering and leaving the settlement area, the rail suffers a slight up-warp. At the position of settlement piers, the mapped deformation of rail shows a gentle and continuous transition curve. The peak values of rail deformation curves provided by ANSYS model and analytical model are both slightly smaller than the pier settlement, further verifying the applicability of analytical model in calculating the mapped relationships between pier settlement and rail deformation. Compared with finite element model, the analytical expression can more intuitively describe the influencing factors of rail deformation and the relationships between various factors and rail deformation as well as save time for ANSYS modeling and calculation.

4. Analysis on influencing factors of rail surface deformation

According to the analytical expression of the mapped relationships between pier settlement and rail deformation, the key factors affecting the bridge-rail mapped relationships can be summarized as the settlement amplitude of pier, settlement type, interlayer stiffness, etc. Based on the verified bridge-track deformation mapped model, studies were conducted on the influencing factors of key parameters such as the settlement amplitude of pier, fastener stiffness, and filling-layer stiffness on the mapped deformation of rail.

Table 1 The material and geometric parameters of different components of the bridge - track system

Components	Materials	Height (mm)	Elastic modulus (GPa)	Poisson's ratio	Moment of inertia (mm^4)	Vertical spring stiffness (N/m)
Rail	U71Mn(K)	176	206	0.3	3.217×10^7	—
Fastener	WJ- 8C	38	—	—	—	3.5×10^7
Track slab	C60 concrete	200	36	0.2	1.65×10^9	—
Filling layer	C40 SCC	90	32.5	0.2	—	1.8×10^9
Base slab	C40 concrete	200	32.5	0.2	1.93×10^9	—
Girder	C50 concrete	3050	34.5	0.2	2.31×10^{13}	—

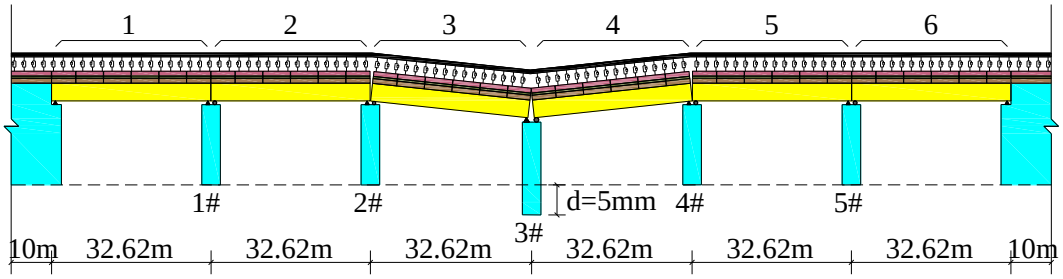

(a) The settlement of single-pier

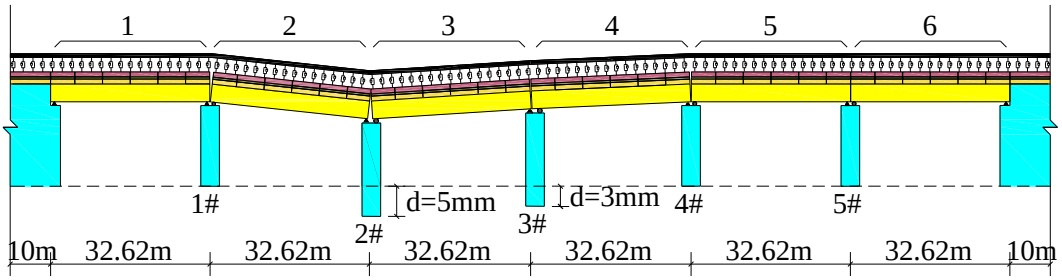

(b) The settlement of two adjacent piers

Fig. 4 Deformation of six-span simply supported bridge during pier settlement

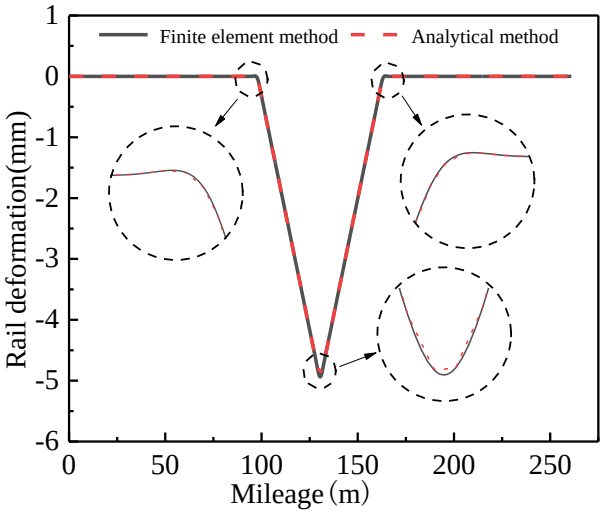

(a) The settlement of single-pier

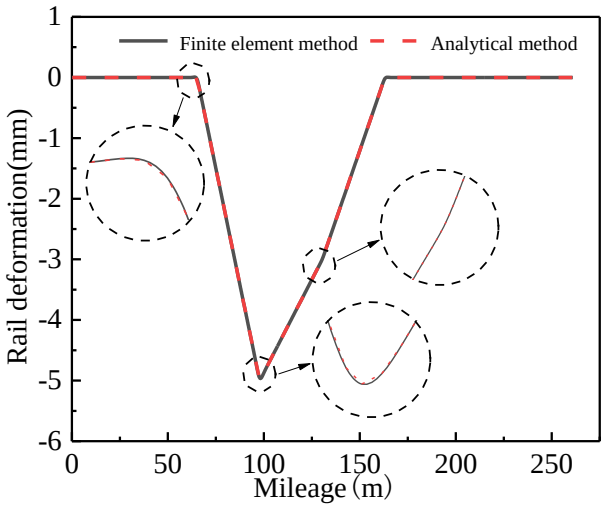

(b) The settlement of two adjacent piers

Fig. 5 The mapped deformation diagram of rail with pier settlement

4.1 Effects of settlement amplitude of pier on mapped deformation of rail surface

To study the variation rules of rail deformation curves of CRTS III SBT - simply - supported bridge with the mode of "longitudinal connection of subgrade, elements on bridge" under different settlement amplitudes of piers, the model of six-span simply - supported bridge with the span of 32.6 m was still taken as an example. Under the conditions of not changing the structure and parameters of bridge, subgrade, and CRTS III SBT, the analytical model was used to calculate the deformation curves of rail with pier settlement when the middle pier suffers five different settlements of 3 mm, 5 mm, 10 mm, 15 mm and 20 mm. The calculation results are shown in Figs. 6 and 7.

When the pier suffers settlement with different amplitudes, the shapes of deformation curves of rail with pier settlement are similar. The larger the pier settlement, the larger the amplitude of rail mapped deformation in the settlement area, the more obvious the up-warp degree of mapped deformation of rail entering and leaving the settlement area, and the greater the formed "angle." The downward and upward mapped deformation amplitudes of rail linearly increase with the increase in pier settlement amplitudes.

The area where the rail deformation exceeds 0.001 mm is defined as the mapped deformation area of rail, and the calculated lengths of these areas corresponding to different settlements are shown in Table 2. The length of rail's mapped deformation area increases with the increase in the amplitude of pier settlement, and it is always slightly longer than the length of two-span beam, because a transition curve will form when the rail enters and leaves the settlement area. According to the relationships among the travelling speed of trains, excitation length of routes, and excitation frequency, the excitation frequency can be expressed as

$$f = \frac{v}{l} \tag{36}$$

Where f is the excitation frequency; v is the travelling speed of trains; l is the excitation length of routes.

When the train passes the rail's mapped deformation area of 24 and 32 m-span bridges at a speed of 200-350 km/h, within the pier settlement range of 3-20 mm, the rail's mapped deformation will cause excitation frequency ranges of 0.99-1.79 Hz for 24 m-span bridge and 0.78-1.39 Hz for 32 m-span bridge, respectively. The excitation frequency caused by rail's mapped deformation at different speeds can be seen in Table 2. These low-frequency excitations are close to the vertical natural vibration frequency (Around 0.8 Hz) of train body (Liu et al. 2020), so it can have a greater influence on the vibration response of train body.

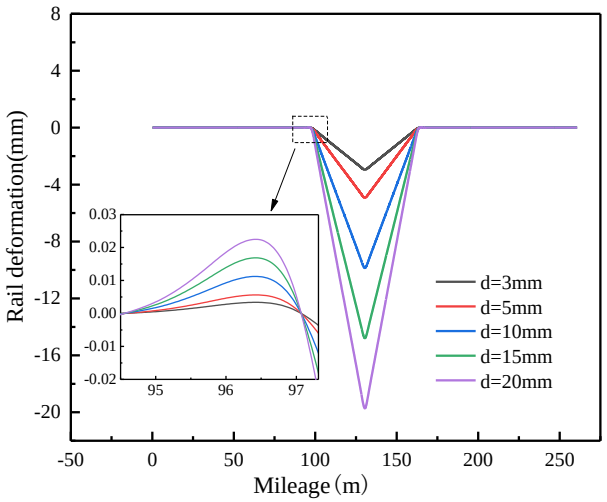

Fig. 6 The mapped deformation diagram of rail under different pier settlements

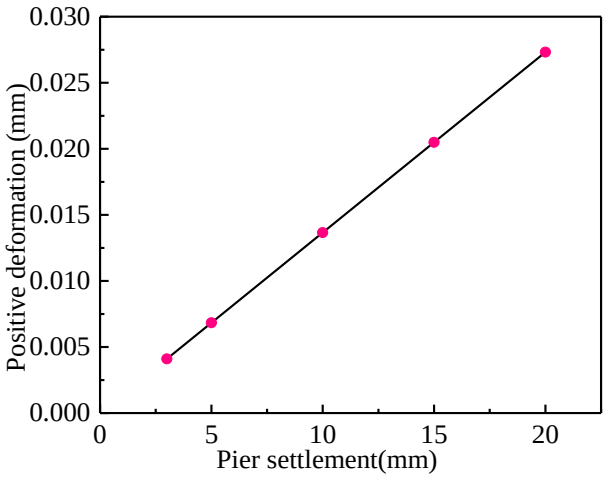

(a) Positive deformation amplitude

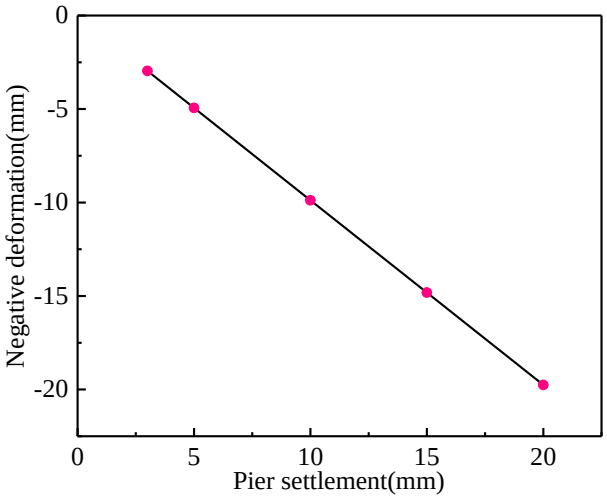

(b) Negative deformation amplitude

Fig. 7 Relationships between the mapped deformation amplitudes of rail and pier settlement

Table 2 Excitation frequency caused by deformation region at different speeds (Unit: Hz)

Settlement (mm)	span (m)	deformation area (m)	Excitation frequency			
			200(km/h)	250(km/h)	300(km/h)	350(km/h)
3	24	54.34	1.022	1.278	1.533	1.789
	32	70.16	0.792	0.990	1.188	1.386
5	24	54.52	1.019	1.274	1.528	1.783
	32	70.47	0.788	0.985	1.183	1.380
10	24	55.60	0.999	1.249	1.499	1.749
	32	70.94	0.783	0.979	1.175	1.370
15	24	55.83	0.995	1.244	1.493	1.741
	32	71.10	0.781	0.977	1.172	1.367
20	24	56.02	0.992	1.240	1.488	1.735
	32	71.26	0.780	0.975	1.169	1.364

4.2 Effects of fastener stiffness on mapped deformation of rail surface

As an important interlayer component connecting rail and track slab, the fasteners will drive the rail to suffer the corresponding deformation when track slabs suffer deformation, thus leading to rail surface irregularity and then affecting the traffic safety of high-speed railway. Based on the verified analytical expression for mapped relationships between pier settlement and rail deformation, fastener stiffness is an important factor affecting the mapped deformation of rail. To quantitatively study the influencing rules of fastener stiffness on the mapped deformation of rail, the model of six-span simply - supported bridge with the span of 32.6 m was still taken as an example under the condition of not changing the structure and parameters of bridge, subgrade, and CRTS III SBT. The analytical model was used to study the rules of rail mapped deformation when the middle pier suffers a settlement of 5 mm for the bridge-track system under five different fastener stiffnesses (10kN/mm, 25 kN/mm, 35 kN/mm, 45 kN/mm, and 55 kN/mm). Fig. 8 shows the mapped deformation curves of rail under five vertical fastener stiffnesses. When the pier suffers a settlement of 5 mm, with the increase in fastener stiffness, the shapes of rail deformation curves are generally identical. At the critical point of rail entering or leaving the settlement area, with the increase in fastener stiffness, the amplitude of positive deformation gradually decreases. At the position where pier settlement occurs, with the increase in fastener stiffness, the amplitude of negative deformation gradually increases. With the increase in fastener stiffness, the length of rail mapped deformation area gradually decreases.

4.3 Effects of SCC filling layer stiffness on mapped deformation of rail surface

To study the effect of SCC filling layer on the mapped relationships between pier settlement and rail deformation, a six-span simply - supported bridge with the span of 32.6 m was still taken as an example. Under the invariable values of other parameters, when the middle pier suffers a settlement of 5 mm, the analytical model was used to investigate the rules of rail mapped deformation in the system under six different vertical stiffnesses of SCC filling layer (1 N/mm^2, 10 N/mm^2, 50 N/mm^2, 100 N/mm^2, 500 N/mm^2, and 1000 N/mm^2).

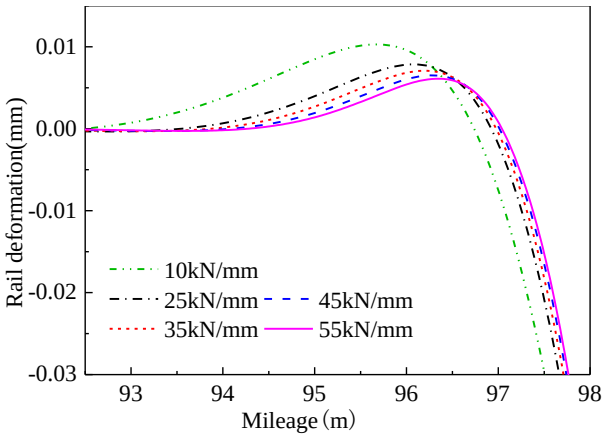

(a) Positive mapped deformation

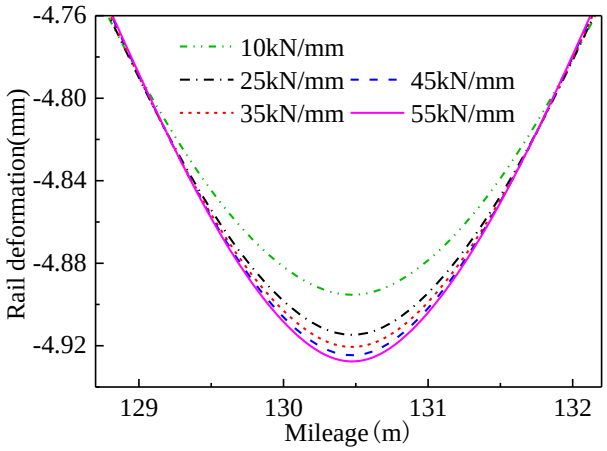

(b) Negative mapped deformation

Fig. 8 The mapped deformation diagram of rail under different fastener stiffnesses

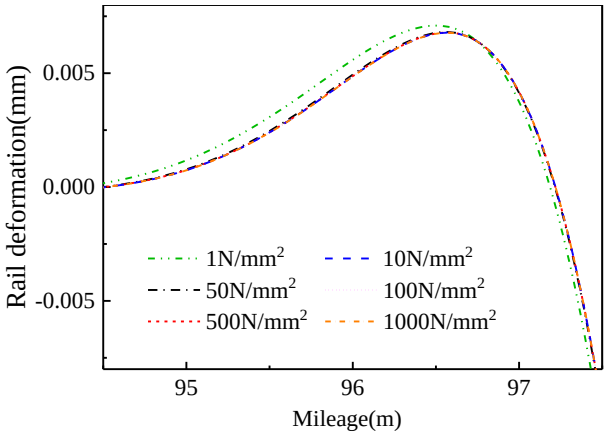

(a) Positive mapped deformation

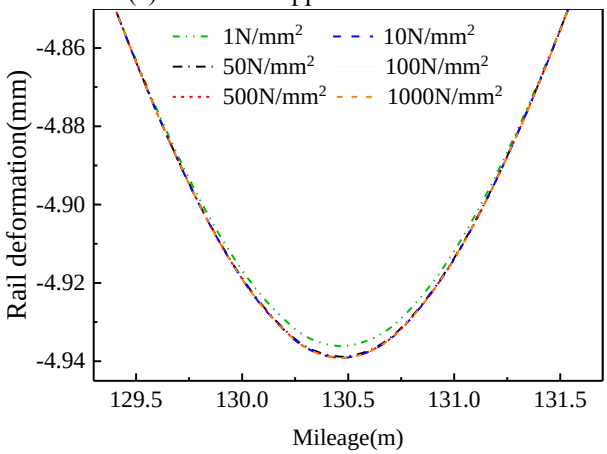

(b) Negative mapped deformation

Fig. 9 The mapped deformation diagram of rail under different stiffnesses of SCC filling layer

Under the six different vertical stiffnesses of SCC filling layer, the calculated mapped deformation curves of rail with pier settlement are shown in Fig. 9. At the settlement of 5 mm, the shapes of rail mapped deformation curves are basically identical under six different vertical stiffnesses of SCC filling layer. With the increase in vertical stiffness of SCC filling layer, the positive deformation amplitude of rail gradually decreases and becomes stable at the rail's boundary points where the rail enters and leaves the settlement area. The negative deformation amplitude of rail at the position of pier settlement gradually increases and becomes stable; meanwhile, the length of mapped deformation area of rail gradually decreases and becomes stable.

5. Conclusions

In this paper, an analytical solution was derived for the mapped relationships between pier settlement and rail deformation in CRTS III SBT-multispan simply - supported bridge system under the mode of non-longitudinal connection ballastless track slab. An ANSYS finite element model was established, and quantitative studies were conducted on the influencing factors and influencing mechanisms of key parameters on the mapped deformation of rail, such as the deformation amplitude of pier settlement, fastener stiffness, and stiffness of SCC filling layer. The following conclusions are drawn:

- The rail's mapped deformation with pier settlement calculated from the analytical solution is basically the same as the numerical solution provided by the finite element model, which verifies the accuracy of analytical method developed in this study. Compared with the finite element model, the analytical model can better describe the relationships between various parameters and rail deformation and save time for ANSYS modeling and calculation.
- The smaller the fastener stiffness, the smoother the mapped deformation curve of rail is, the greater the length of rail's mapped deformation area is, and the less obvious the track irregularity is.
- The mapped deformation of rail caused by the pier settlement of common-span bridge structures will generate low-frequency excitation on high-speed trains. The frequency of low-frequency excitation is close to that of vertical natural vibration of train body, which will significantly affect the vibration of train body.
- With the increase in vertical stiffness of SCC filling layer, the amplitude of rail's positive deformation gradually decreases and becomes stable at the boundary points of rail entering and leaving the settlement area. Meanwhile, the length of the mapped deformation area of rail gradually decreases and becomes stable.

Acknowledgments

The research described in this paper was financially supported by the National Natural Science Foundation of China (51778630, U1934207), Hunan Innovative Provincial Construction Project (2019RS3009).

References

Ahmari, S., Yang, M.J. and Zhong, H. (2014), "Dynamic interaction between vehicle and bridge deck subjected to support settlement", *Eng. Struct.*, **84**, 172-183. http://dx.doi.org/10.1016/j.engstruct.2014.11.018.

Al Shaer, A., Duhamel, D., Sab, K., Foret, G. and Schmitt, L. (2008), "Experimental settlement and dynamic behavior of a portion of ballasted railway track under high speed trains", *J. Sound Vib.*, **316**(1-5), 211-233. https://doi.org/10.1016/j.jsv.2008.02.055.

Biondi, B., Muscolino, G. and Sofi, A. (2005), "A substructure approach for the dynamic analysis of train–track–bridge system", *Comput. Struct.*, **83**(28-30), 2271-2281. https://doi.org/10.1016/j.compstruc.2005.03.036.

Cai, C.S., Shi, X.M., Voyiadjis, G.Z. and Zhang, Z.J. (2005), "Structural performance of bridge approach slabs under given embankment settlement", *J. Bridge Eng.*, **10**(4), 482-489. https://doi.org/10.1061/(ASCE)1084-0702(2005)10:4(482).

Chen, Z.W., Zhai, W.M. and Tian, G.Y. (2018), "Study on the safe value of multi-pier settlement for simply supported girder

bridges in high-speed railways", *Struct. Infrastruct. E.*, **14**(3), 400-410. https://doi.org/10.1080/15732479.2017.1359189.

Chen, Z.W., Zhai, W.M., Cai, C.B. and Sun, Y. (2015), "Safety threshold of high-speed railway pier settlement based on train-track-bridge dynamic interaction", *Science China Technological Sciences.*, **58**(2), 202-210. https://doi.org/10.1007/s11431-014-5692-0.

Doménech, A., Museros, P. and Martínez-Rodrigo, M.D. (2014), "Influence of the vehicle model on the prediction of the maximum bending response of simply - supported bridges under high-speed railway traffic", *Eng. Struct.*, **72**, 123-139. https://doi.org/ 10.1016/j.engstruct.2014.04.037.

Erol, B.A. (2018), "Finite element model calibration of a steel railway bridge via ambient vibration test", *Steel Compos. Struct.*, **3**(27), 327-335. https://doi.org/ 10.12989/scs.2018.27.3.327.

Gong, X. and Li, Z. (2016), "Bridge pier settlement prediction in high-speed railway via autoregressive model based on robust weighted total least-squares", *Surv Rev.*, **50**(359), 147-154. https://doi.org/10.1080/00396265.2016.1236162.

Gou, H.Y., Ran, Z.W., Yang, L.C., Bao, Y. and Pu, Q.H. (2019), "Mapping vertical bridge deformations to track geometry for high-speed railway", *Steel Compos. Struct.*, **32**(4), 467-478. https://doi.org/10.12989/scs.2019.32.4.467.

Guan, M.S., Liu, W.T., Lai, M.H., Du, H.B., Cui, J. and Gan, Y.Y. (2019), "Seismic behaviour of innovative composite walls with high-strength manufactured sand concrete", *Eng. Struct.*, **195**, 182-199. https://doi.org/10.1016/j.engstruct.2019.05.096.

Indraratna, B., Ngo, N.T., Rujikiatkamjorn, C. and Vinod, J.S. (2014), "Behavior of fresh and fouled railway ballast subjected to direct shear testing: Discrete element simulation", *Int. J. Geomech.*, **14**(1), 34-44. https: //doi.org/ 10.1061/(ASCE)GM.1943-5622.0000264.

Jahangiri, M. and Zakeri, J.A. (2017), "Dynamic analysis of train-bridge system under one-way and two-way high-speed train passing", *Struct. Eng.*, **64**, 33-44. https: //doi.org/ 10.12989/sem.2017.64.1.033.

Jiang, L.Z., Chai, X.L, Tan, Z.H., Zhou, W.B., Feng, Y.L., Lai, Z.P and Zheng, L. (2019), "Dynamic analyses of a simply supported double-beam system subject to a moving mass with fourier transform technique", *Comput. Model. Eng. Sci.*, **121**(1), 291-314.

Jiang, L.Z., Feng, Y.L, Zhou, W.B. and He, B.B. (2019), "Vibration characteristic analysis of high-speed railway simply supported beam bridge-track structure system", *Steel Compos. Struct.*, **31**(6), 591-600. https://doi.org/10.12989/scs.2019.31.6.591.

Ju, S.H. (2013), "3D analysis of high-speed trains moving on bridges with foundation settlements", *Arch. Appl. Mech.*, **83**(2), 281-291. https://doi.org/10.1007/s00419-012-0653-1.

Liu, X., Xiang, P., Jiang, L.Z., Lai, Z.P., Zhou, T. and Chen, Y.J. (2019), "Stochastic Analysis of Train-bridge System Using the Karhunen-Loeve Expansion and the Point Estimate Method", *Int J Struct Stab Dy.*

Liu, X., Jiang, L.Z., Lai, Z.P., Xiang, P. and Chen, Y.J. (2020), "Sensitivity and dynamic analysis of train-bridge coupled system with multiple random factors", *Eng. Struct.*, **221**, 111083. https://doi.org/ 10.1016/j.engstruct.2020.111083.

Lee, J.S., Choi, S., Kim, S., Kim, Y.G., Kim, S.W. and Park, C. (2012), "Waveband analysis of track irregularities in high-speed railway from on-board acceleration measurement", *J. Solid Mech. Mater. Eng.*, **6**(6), 750-759. https://doi.org/ 10.1299/jmmp.6.750.

Niu, F.J., Lin, Z.J., Lu, J.H., Liu, H. and Xu, Z.Y. (2011), "Characteristics of roadbed settlement in embankment–bridge transition section along the Qinghai-Tibet Railway in permafrost regions", *Cold Reg Sci Technol*, **65**(3), 437-445. https://doi.org/10.1016/j.coldregions.2010.10.014.

Paixão, A., Fortunato, E. and Calçada, R. (2015), "The effect of differential settlements on the dynamic response of the train–track system: A numerical study", *Eng. Struct.*, **88**, 216-224. http://dx.doi.org/10.1016/j.engstruct.2015.01.044.

Rocha, J.M., Henriques, A.A., Calçada, R. and Rönnquist, A. (2015), "Efficient methodology for the probabilistic safety assessment of high-speed railway bridges", *Eng. Struct.*, **101**, 138-149.https://doi.org/ 10.1016/j.engstruct.2015.07.020.

Shan, D.S., Cui, S.G. and Huang, Z. (2013), "Coupled vibration analysis of vehicle-bridge system based on multi-boby dynamics", *J. Transportation Technologies,* **03**(02), 1-6. http://dx.doi.org/10.4236/jtts.2013.32A001.

Toydemir, B., Kocak, A., Sevim, B. and Zengin, B. (2017), "Ambient vibration testing and seismic performance of precast I beam bridges on a high-speed railway line", *Steel Compos. Struct.*, **23**(5), 557-570. https://doi.org/ 10.12989/scs.2017.23.5.557.

Wang, P., Wei, K., Wang, L. and Xiao, J. (2015), "Experimental study of the frequency-domain characteristics of ground vibrations caused by a high-speed train running on non-ballasted track", Proceedings of the Institution of Mechanical Engineers, Part F: *Journal of Rail and Rapid Transit*, **230**(4), 1131-1144. https://doi.org/10.1177/0954409715577849.

Wang, Y.J., Wei, Q.C. and Yau, J.D. (2013), "Interaction response of train loads moving over a two-span continuous beam", *Int. J. Struct. Stab. Dy.*, **13**(1), 1350002. https://doi.org/10.1142/S0219455413500028.

Xia, H., Zhang, N. and Guo, W.W. (2006), "Analysis of resonance mechanism and conditions of train–bridge system", *J Sound Vib*, **297**(3-5), 810-822. https://doi.org/10.1016/j.jsv.2006.04.022.

Xiong, J.Z., Yu, H.B. and Gao, M.M. (2006), "Effect of pier and abutment non-uniform settlement on train running behavior", *Computational Methods In Engineering And Science*, Berlin, Heidelberg.

Yan, W.J., Zhao, M.Y., Sun, Q and Ren, W.X. (2018), "Transmissibility-based system identification for structural health monitoring: fundamentals, approaches, and applications", *Mech. Syst. Signal Pr.*, https://doi.org/10.1016/j.ymassp.2018.06.053.

Yang, Q., Leng, W.M., Zhang, S., Nie, R.S., Wei, L.M., Zhao, C.Y. and Liu, W.Z. (2014), "Long-term settlement prediction of high-speed railway bridge pile foundation", *J. Cent. South Univ*, **21**(6), 2415-2424. https://doi.org/10.1007/s11771-014-2195-x.

Yang, Y.B. and Yau, J.D. (2017), "Resonance of high-speed trains moving over a series of simple or continuous beams with non-ballasted tracks", *Eng. Struct.*, **143**, 295-305. http://dx.doi.org/10.1016/j.engstruct.2017.04.022.

Yau, J.D. (2009), "Dynamic response analysis of suspended beams subjected to moving vehicles and multiple support excitations", *J. Sound Vib.*, **325**(4-5), 907-922. https://doi.org/10.1016/j.jsv.2009.04.013.

CC